BioNanoScience (2026) 16:25
https://doi.org/10.1007/s12668-025-02288-5

RESEARCH

Micro-Rheology and Co-Stream Microfluidics Reveal Critical Contributions of Platelet Concentrate Components to Blood Platelet Integrity in Storage

Dean Pym[1,2] · Alison Paul[3] · Amanda J. Davies[1] · Jessica O. Williams[1] · Christine Saunders[2] · Chloë E. George[2] · Philip E. James[1]

Received: 5 August 2025 / Accepted: 3 November 2025

Abstract
Fluid viscosity is important in both physical and biological systems, as it helps describe a fluid's material properties. Recent findings show that the shear stress experienced during storage of blood products can result in damage of platelets making the viscosity of stored platelet concentrates (PC) an important area of study. In this work we characterised the contribution of different components of the PC to viscosity using nanoparticle tracking microrheometry and co-stream microfluidics, to determine whether reduced viscosity approaches can improve PC quality over storage. Validation experiments showed both methods could accurately report on the viscosity of samples, with the microfluidics approach deemed preferable due to the possibility of changing flow rates and therefore studying a range of shear stress. PC quality was assessed over 8 days by measuring platelet count, mean platelet volume (MPV), platelet distribution width (PDW), pH, aggregation, and platelet activation markers. Results showed that PC viscosity depends on the residual plasma following processing and is independent of the stored platelet concentration. Reducing plasma to 10% maintained PC quality over 8 days, but further plasma reductions led to reduced platelet counts and increased MPV by day 8. Platelet function, including aggregation and activation, were similar with plasma levels $\geq$ 10%. This study concludes reduced plasma strategies for PC have limited influence on mitigating shear induced platelet deterioration over storage.

Keywords Microfluidics · Platelet Concentrate · Rheology · Nanoparticle Tracking · Shear Stress

1 Introduction

Platelet (PLT) concentrates (PCs) are a critical blood component used in transfusion medicine to therapeutically manage bleeding in patients or as prophylaxis in patients with thrombocytopenia. PCs are stored under controlled conditions for up to 7 days, during which they must retain adequate viability and functionality. Unlike other blood components, PCs are stored at room temperature (22 °C ± 2 °C), with continuous gentle agitation to preserve metabolic activity. They are highly sensitive to their physical and biochemical environment and storage induced stresses can lead to a range of deleterious changes collectively known as the PLT storage lesion (PSL) [1]. These changes include a loss of their discoid shape [2, 3], PLT activation [4] and the subsequent shedding of key adhesion receptors such as the thrombin receptors PAR1 and PAR4, GPVI and GP1bα (collagen and von Willebrand factor receptors, respectively) [5–7]. These changes ultimately reduce the therapeutic efficacy of PCs as a transfusion product. As our understanding of PLT biology has advanced, increased attention has been directed toward the mechanical factors influencing PLT quality over storage, particularly shear forces encountered during collection, processing, and maintenance [8, 9].

✉ Dean Pym
dpym@cardiffmet.ac.uk

1 Cardiff Metropolitan University, Centre of Cardiovascular Research, Innovation and Development (CURIAD), Llandaff Campus, Western Ave, Cardiff CF5 2YB, UK

2 Welsh Blood Service, Component Development and Research Laboratory, Ely Valley Rd, Talbot Green, Ynysmaerdy, Pontyclun CF72 9WB, UK

3 School of Chemistry, Cardiff University Main Building, Park Place, Cardiff CF10 3AT, UK

Published online: 17 December 2025

The shear induced PSL (Si-PSL) refers to the deleterious changes that occur due to shear exposure, from the point of blood withdrawal to the time of transfusion. The term 'shear' is described by both the shear rate and the shear stress. Shear rate refers to the rate and duration of flow, described by change in velocity between two adjacent fluid microlayers divided by their distance. While shear stress refers to the magnitude of tangential force applied coplanar to the flow region [10, 11]. Fluid viscosity is the measure of a fluid's resistance to flow and specifies the coefficient of proportionality between the shear rate and shear stress. For a solid, the shear stress is dependent on the deformation itself [12], while for a liquid, shear stress is a function of the rate of strain. As shear rate (dv/d h) is a function of both fluid speed and the height above the given boundary, shear stress can be described as -μ(dv/d h), where μ is dynamic fluid viscosity, ν is fluid speed, and h is the height above the face of a material [13].

A study by Pym et al. [14], investigated how the different components of shear rate influence PC quality over storage [14]. The study highlighted that storage in reduced volume containers increased shear exposure though changes to h, which was associated with increased activation and reduced functionality over eight days of storage. This supported work by Schoenfeld et al. [15], demonstrating excess spontaneous PLT activation following reduced volume storage and reduced ADP-induced activation [15]. The loss of PC quality observed over storage in reduced volume containers was partially resolved by adjusting the agitation frequency (ν), with storage at 20 rpm showing improved functionality in early storage and storage at 40 rpm showing improvements in activation and functionality over the storage duration, compared to storage at 60 rpm [14]. The above observations were preceded by an earlier study by Shankaran et al. [16], showing PLT activation was greater effected by the extent of constant shear applied to the suspension rather than temporal variations in shear. Likewise, the study indicated shear induced PLT activation is governed by the magnitude of the force exerted on the suspension, as increasing the suspension viscosity 2-fold at a constant shear rate led to a 3.3-fold rise in PLT activation [16]. Therefore, it has been hypothesised that reduced viscosity approaches could provide an alternative route to address the Si-PSL by reducing the magnitude of force induced on a fluid at a given shear rate.

An important consideration in this context is the ratio of residual plasma to platelet additive solution (PAS) used for storage. Most transfusion services use a 65% PAS to 35% plasma to balance the supply of glucose, coagulation factors, and key plasma proteins with the buffering benefits of PAS [17, 18]. However, little is known about how this ratio influences mechanical properties such as shear stress and viscosity. Material viscosity measurements have shown promise for effectively monitoring variations in physiological and pathological conditions [19, 20]. The current methods for rheological characterisation of biological samples typically fall into three categories: capillary [21], rotating [22], and falling ball type [23]. These approaches are limited by the repetitive and time-consuming testing required, leading to large sample consumption and inefficiency. With this, several microrheometric devices have been proposed due to their advantages over conventional bulk viscometric testing. This includes small sample volume consumption, where rotating type and falling ball type methods requiring tens of millilitres of sample [24, 25], whereas capillary type and microrheological methods typically only require between 10 and 200ul sample volumes [26]. Other advantages of microrheometric devices include ease of use, high through-put capacity, and disposability, highlighting their potential for automation and used in point-of-care testing [27]. This study aimed to utilise these microfluidic models to characterise the rheological properties of stored PCs to highlight areas which could address the Si-PSL and optimise the therapeutic stored PC product for transfusion. Rheological characterisation was followed by assessments of PLT viability, morphology, surface expression and functionality, over eight days of storage.

2 Methods

2.1 Sample Preparation

Sucrose suspensions were prepared fresh before use to ensure stability and kept in sterile containers to prevent contamination. Sucrose (cat: AA3650830, Fisher Scientific) was suspended in distilled water to yield concentrations between 0–30% (w/wt.). Suspensions were mixed until the sucrose was fully dissolved.

Buffy coats (BC) were collected from whole blood donations kept at 22 °C±2 °C without agitation overnight in accordance with the JPAC guidelines [28]. Four ABO specific BC were pooled with 250 ml of SSP+™ PAS (Macopharma, Moureaux, France), providing a PAS to plasma ratio of approximately 65:35. The BC pools were centrifuged at 500 g for 8 min at 22 °C (Sorvall RC12BP+,Thermo Scientific, United States), and the plasma/PAS, comprising the PC, separated from the remaining red blood cells using a blood component separator (CompoMat G5+, Fresenius Kabi, Germany). This simultaneously leucodepleted the PC through an integral white cell reduction filter (Autostop™; Haemonetics, Boston MA, USA) to provide a pooled PC (290–310 ml). Pooled PCs were subsequently split into neonatal PC storage bags (VQE605B, Macopharma, France) to create four neonatal PCs (50–70 ml). For reduced plasma storage, PCs (50–70 ml) were subsequently centrifuged at 800 g for 10 min and resuspended in different ratios of PAS

to plasma. PAS was supplemented with 1 mg/ml dextrose monohydrate (cat: D9559, Sigma-Aldrich). PCs were then stored at 22 °C ± 2 °C with constant 60 rpm agitation with a horizontal displacement of ± 2.5 cm for 8 days. PLT concentration ([PLT]) for rheological analysis was modified by centrifugation. PCs were centrifuged at 800 g for 10 min to isolate the cell pellet. Pellets were resuspended in 0.5x, 1x, or 2 × their original suspension volume to yield 2x, 1x, or 0.5x [PLT], respectively.

Fresh frozen plasma (FFP) was separated from PLTs by a subsequent centrifugation at ~ 2500 g for 15 min at 22 °C (Sorvall RC12BP+, Thermo Scientific, United States), followed by separation using a blood component separator (CompoMat G5 +, Fresenius Kabi, Germany). FFP preparations were diluted in PAS to yield concentrations (PAS:plasma) as follows: 100% plasma (0:1), 75% plasma (1:3), 50% plasma (1:1), 25% plasma (3:1), and PAS only (1:0). To ensure visual clarity for nanoparticle tracking microrheometry (NTM), FFP and PC supernatant underwent ultracentrifugation at 100,000 g for 60 min at 4 °C using a Sorvall Discovery 100SE ultracentrifuge (Hitachi, Japan).

2.2 Haematology Analysis

Full blood counts (FBC) from PC and FFP (including red blood cell (RBC), white blood cell (WBC), and PLT counts) were measured using the ABX Pentra XL80 Haematology Analyzer (HORIBA, United Kingdom). Using the individually reported cell counts, the cell components of the PC suspension can be reported as volume fractions (Ø). Simply, $Ø_{Total} = Ø_{RBC} + Ø_{PLT} + Ø_{WBC}$ (where, $Ø_{WBC} = Ø_{neutrophil} + Ø_{lymphocyte} + Ø_{eosinophil} + Ø_{monocyte} + Ø_{basophil}$) [29]. Volume fractions were calculated using the cell counts and the corresponding average cell volume for each cell type (Table 1). PLT count and MPV were also reported on day 1, and day 8 of storage. pH was measured directly from fresh PLT samples using a HORIBA LAQUAtwin pH meter, which was calibrated (2-point) prior to use.

2.3 Nanoparticle Tracking Microrheometry

Nanoparticle tracking analysis (NTA) is a method used for characterisation and quantification of particles with a diameter of 10–1000 nm. This technique tracks the Brownian motion of individual particles over a defined timeframe using a × 20 magnification microscope, while the particles interact with a 405 nm laser (Fig. 1), as described elsewhere [30–32]. Brownian motion is analysed using the Stokes–Einstein equation (Eq. 1.1).

$$D = \frac{K_b T}{3\pi\mu r} \tag{1.1}$$

Table 1 PC cell counts and volume fractions for PC suspensions

Sample	PLT		RBC		WBC		Total	
	Count ($\times 10^9$/L)	$Ø_{PLT}$ (%)	Count ($\times 10^9$/L)	$Ø_{RBC}$ (%)	Count ($\times 10^9$/L)	$Ø_{WBC}$ (%)	Count ($\times 10^9$/L)	$Ø_{Total}$ (%)
PAS	0	0	0	0	0	0	0	0
PC1	1111	1.089	40	0.200	0.2	< 0.001	1151.2	1.289
PC2	1030	1.009	40	0.348	0.1	< 0.001	1080.1	1.357
PC3	1187	1.163	30	0.348	0.1	< 0.001	1217.1	1.511
PC4	1050	1.029	30	0.261	0.1	< 0.001	1080.1	1.311

Reported values denote raw cell count and calculated volume fractions. PC replicates were denoted as PC1-PC4

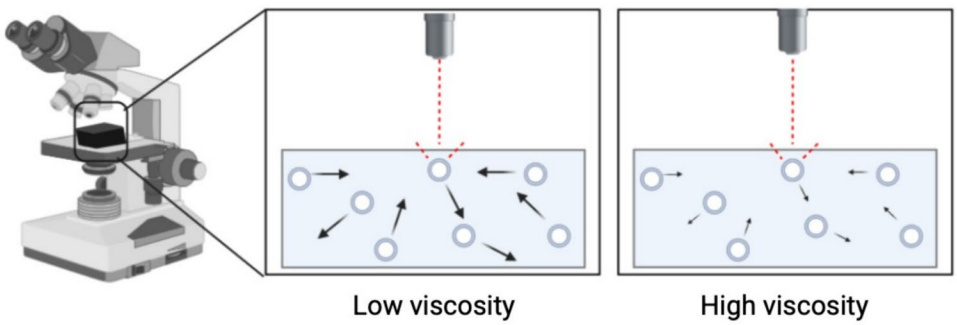

Fig. 1 Principles of Nanoparticle Tracking microrheometry. Schematic representation of the observed Brownian motion in different suspension media. In a low viscosity suspension (left), particles exhibit high mobility, resulting in increased Brownian motion. In a high viscosity suspension (right), particle movement is reduced, decreasing Brownian motion. The red lines indicate light scattering observed under the microscope

where D is the diffusion coefficient computed using the mean square of particle movement, K_b is the Boltzmann constant, T is temperature, μ is the viscosity, and r is the particle radius. For fluid viscosity approximations, the Stokes–Einstein equation can be rearranged to Eq. 1.2.

$$\mu = \frac{K_b T}{3\pi D r} \tag{1.2}$$

If $K_{b,}$ T, and r, are constant, an increase or decrease in viscosity results in a decrease or increase in Brownian motion, respectively. This will change the apparent (measured) bead diameter recorded in the test suspension. The relationship between the ratio of the measured and reference bead diameter, to the ratio of the measured and reference viscosity can be described as Eq. 1.3.

$$\frac{\mu_{Test}}{\mu_{reference}} = f\left(\frac{r_{Test}}{r_{reference}}\right) \tag{1.3}$$

Fluid viscosity approximation was done using a Nanosight LM10 (NTA 3.4, Malvern Panalytical, UK). Polyethylene beads (Bangs Laboratories Inc, cat: 832) of a known diameter (reference: 200 nm) were suspended in test suspensions at 22 °C, at bead concentrations between 1×10^6 and 1×10^9 particles/ml. Flow was induced by syringe pump (Harvard Apparatus, Cat: 98–4730). Five 30 s frames were captured and analysed using the NTA software (Malvern Panalytical, UK).

2.4 CO-STREAM Microfluidics

Co-stream microfluidic rheometry works by tracking the interface between dual flowing laminar streams (Re< <2300) as described in similar studies [27, 33, 34]. A microfluidic "Y shaped" channel was proposed to measure viscosity at a range of shear rates, allowing individual inlets for a test sample and a reference sample. Using the Hagen-Poiseuille equation (Eq. 2.1), the pressure of a single laminar stream is proportional to the flow rate and viscosity of the fluid, at constant channel geometries.

$$P = \frac{128\mu Q \Delta L}{\pi D^4} \tag{2.1}$$

where *P* is the pressure, Q is the flow rate, ΔL is the change in length, and D is the diameter. *As* ΔL, π and D, are constant, Eq. 2.1 can be simplified to $P \propto \mu Q$. Therefore, the pressure ratio between the dual flowing streams within the comparator region of the microfluidic channel, the test (P_{test}) and reference (P_{ref}) fluid, can be described as Eq. 2.2 where $f(W/W_{total})$ denotes a function of the interface location.

$$\frac{PTest}{PRef} = \frac{\mu Test}{\mu Ref}\frac{QTest}{QRef} = f\left(\frac{W}{Wtotal}\right) \tag{2.2}$$

Microfluidic device design was performed using Autodesk Fusion 360 (Autodesk, USA) and fabricated by BEOn-Chip (Spain). The channel consists of a comparator region (W:2 mm, L:28.66 mm, H:100 μm), and two inlet channels (W:1 mm, L:15.38 mm, H:100 μm); one for test fluid (Q = 25–400 μl/min) and one for the reference fluid (Q = 100 μl/min) consisting of PBS with 0.01% trypan blue (BDH Chemicals Ltd, C.I: 23850). To evaluate the dependency of shear rate on viscosity, the pressure ratio (1:1) was kept constant, while the flow rate between both inlets was changed between 10–750 μl/min. Inlet channels were sufficiently long to ensure the fluid profile was fully developed. Fluid flow was initiated using FlowEZ pressure based microfluidic pumps (Fluigent, France) and flow was captured using a Nikon Ts2 Eclipse optical microscope (Nikon, Japan) mounted with a 75 FPS INFINITY 5 camera (Teledyne Lumenera, Canada) (Fig. 2). Interface location (W/W_{total}) was analysed using ImageJ [35].

2.5 PLT Aggregation

PLT aggregation was evaluated using the Multiplate® multiple electrode aggregometry system (Roche Diagnostics Ltd, Switzerland), following a previously published protocol [14]. PCs were first mixed in a 2:1 ratio with SSP+™ PAS, then further diluted 1:1 with either 0.9% Sodium Chloride (NaCl; for ristocetin stimulation) or 0.9% NaCl supplemented with 3 mM Calcium Chloride ($CaCl_2$; for TRAP-6 stimulation). All reagents were prewarmed to 37 °C, in line with the manufacturer's guidelines. During measurement, a Teflon-coated stir bar ensured constant mixing. Aggregation was triggered by the addition of either ristocetin (50 μL; final concentration 0.77 mg/mL) or TRAP-6 (20 μL; final concentration 32 μM) (both from Roche Diagnostics Ltd, Switzerland). Electrical impedance was recorded continuously for 6 min, and results were quantified as the area under the curve (AUC).

2.6 Flow Cytometry

Flow cytometry was then used to determine CD41+/CD62P+and CD41+/CD42b+expression, using on the Cytoflex flow cytometer (Beckman coulter), as described elsewhere [14]. The antibodies used were as follows: APC conjugated anti-CD41a (BD Pharmingen™, cat: 559777), FITC conjugated anti-CD62P (BD Pharmingen™, cat: 555523), PE conjugated anti-CD42b (Abcam, cat: AB232912), APC conjugated IgG1 (BD Pharmingen™, cat: 555751), FITC conjugated IgG1 (BD Pharmingen™, cat: 555748), and PE conjugated IgG1 (BD Pharmingen™, cat:555749).

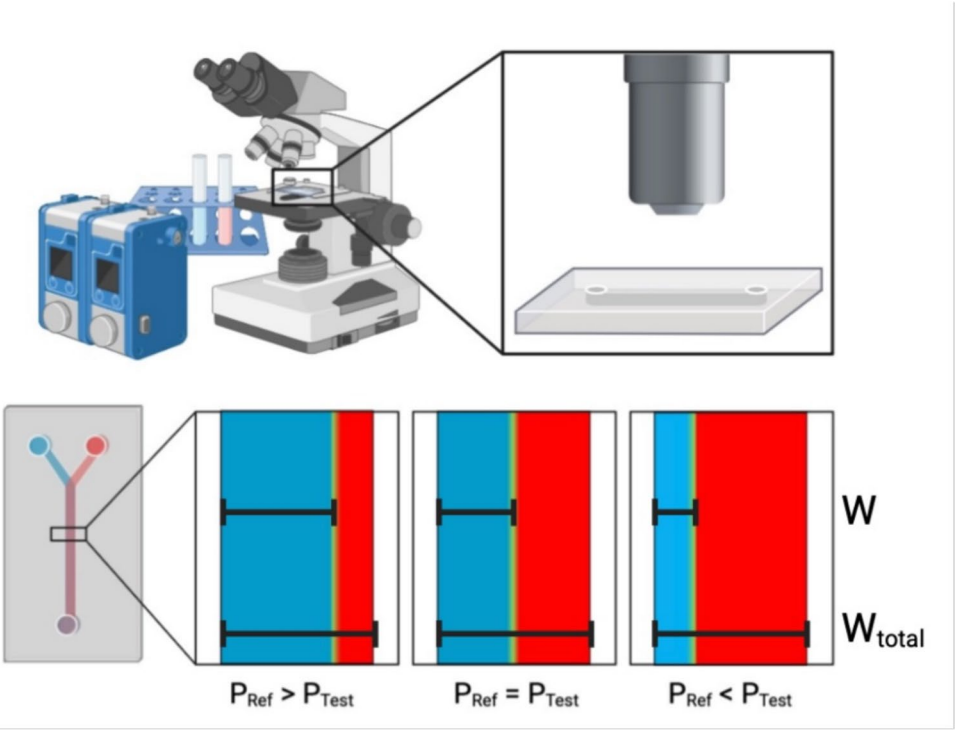

Fig. 2 Principle of co-stream microfluidic rheometry. Co-flow microfluidic approach for measuring relative viscosity between two fluids. A reference fluid (blue) and a test fluid (red) are introduced to the co-stream 'Y' shaped channel using pressure-based microfluidic pumps, and the interface between fluids is visualised under a microscope. The location of the interface relative to the total width (W/W_{total}) reflects the differences in pressure, proportional to the differences in viscosities ($P \propto \mu Q$), between the reference and test fluid

2.7 Statistical Analysis

Data analysis was completed using GraphPad Prism 9 software (San Diego, USA). Statistical significance was inferred by either simple linear regression, non-linear regression, or a two-way ANOVA followed by a post hoc Tukey's test. A P value of <0.05 was considered statistically significant.

3 Results

3.1 NTM model Calibration

NTM was calibrated using 0–20% (w/wt.) sucrose-water suspensions, a concentration range that represents viscosities of ~ 1 cP to ~ 2 cP, overlapping with normal plasma viscosity (~ 1.4–1.8 cP) [36]. As expected, the observed bead diameter increased with increased suspension viscosity (Fig. 3A, B), indicating the model's sensitivity to fluid viscosity. The relationship between $\mu_{test}/\mu_{reference}$ to $D_{test}/D_{reference}$ was assessed using simple linear regression. The simple linear regression analysis gave the fitting line described by $Y=X+0.0$ with an $R^2>0.97$ (Fig. 3C, confirming a strong linear relationship; so, Eq. 1.4 can be reliably used to approximate the viscosity of the test fluid based on bead diameter measurements. Using this calibration, NTM determined the viscosity of sucrose suspensions as follows: 10% sucrose = 1.434 cP (95% CI: 1.359–1.510) and 20% sucrose = 1.875 cP (95% CI: 1.682–2.069).

$$\mu_{Test} = \frac{d_{Test}\mu_{reference}}{d_{reference}} \tag{1.4}$$

3.2 Co-Stream Microfluidics Calibration

The relationship between the P_1/P_2 and W/W_{total} for the co-stream microfluidic model was calculated before use and determined by non-linear regression analysis (Fig. 4A). The regression analysis used a fitting line of $Y=A1*X^{B1}+C1*X^{D1}$. Example fitting values as follows: A1 = 3.566, B1 = 1.803, C1 = 18.27, and D1 = 11.68 ($R^2>0.99$).

$$\frac{P_1}{P_2} = 3.566 * X^{1.803} * 18.27 * X^{11.68} \tag{2.3}$$

To calibrate the model to measure the dependency of shear rate on viscosity, the flow rate from both inlets was kept equal and adjusted between 10–750 µl/min, to maintain a pressure ratio of 1:1 with varying the flow rate (Fig. 4B). The regression analysis used a fitting line of $Y=A2+B2*X+C2*X^2$ and provided fitting values such as: A2 = 0.497, $B2=-1.242\times10^{-4}$, and $C2=-1.018\times10^{-7}$

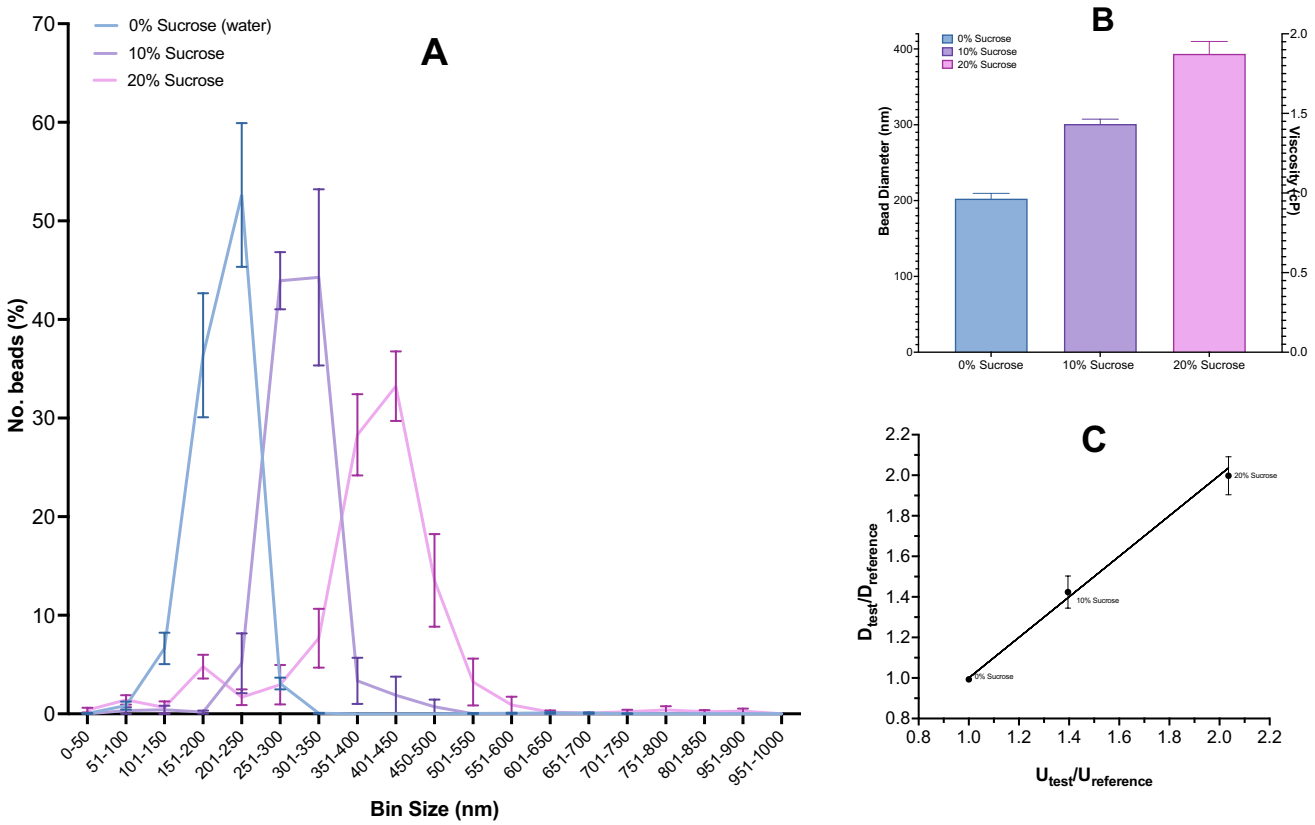

Fig. 3 NTM for the approximation of fluid viscosity. (**A**) shows the measured bead size distribution of 200 nm beads suspended in different sucrose solutions. (**B**) shows the average apparent bead diameter and calculated viscosity in different sucrose suspensions. (**C**) the relationship between the $U_{test}/U_{reference}$ to $D_{test}/D_{reference}$. The black line denotes the fitting lines given by linear regression. Data is presented as mean values with error bars representing standard deviation (SD)

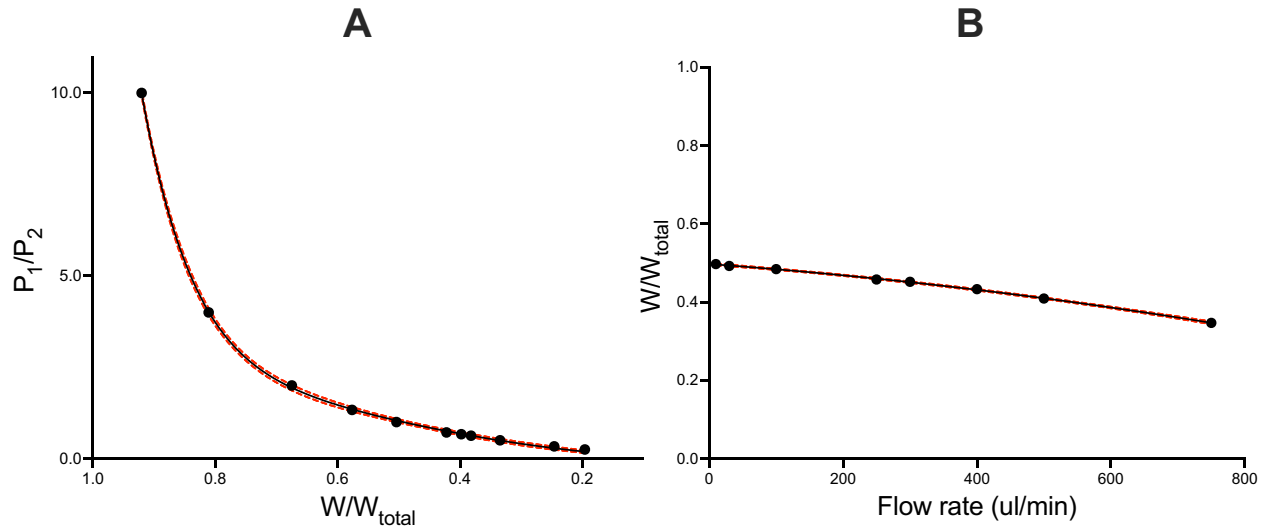

Fig. 4 Co-stream microfluidic model validation for rheological characterisation. (**A**) shows the line fitting for P1/P2 against W/W_{total} (**B**) Fitting line for flow rate against W/W_{total} when P1 = P2. The black line denotes the fitting lines given by non-linear regression, and the 95% confidence intervals are represented by the red dotted lines

($R^2 > 0.99$). This step highlighted an adjusted W/W_{total} was required to replace 'X' in Eq. 2.3. This can be calculated by Eq. 2.4, where X_{actual} is the experimental flow rate, and X_{100}, is a flow rate of 100 µl/min set as a constant for comparison.

$$\left(\frac{W}{W_{total}}\right)_{adjusted} = \left(\frac{W}{W_{total}}\right)_{Measured} + B2\left(X_{100} - X_{actual}\right) + C2\left(X_{100}^2 - X_{actual}^2\right) \quad (2.4)$$

3.3 Co-Stream Microfluidics Validation

To ensure that the adjustment (Eq. 2.4) maintained the expected viscosity-pressure relationship, the viscosity of 30% sucrose (w/wt.) was measured with and without the adjustment to W/W_{total} (Fig. 5A). Linear regression analysis demonstrated that the correction significantly improved the consistency of the viscosity-pressure relationship. The gradient obtained with the adjustment was 3.207 (95% CI: 3.166–3.249), which is consistent with the expected viscosity at 30% sucrose. The gradient without the adjustment was 4.012 (95% CI: 3.721–4.304), indicating that the uncorrected data overestimated viscosity.

The co-stream channel was also shown to maintain accurate viscosity measurements over a range of shear rates (Fig. 5B). Simple linear regression analysis showed no significant difference between the slopes (F (DFn, DFd) = 1.005. (2, 3), $P = 0.4632$), and were significantly zero for 10% sucrose (F (DFn, DFd) = 3.2 (1, 1), $P = 0.3245$, $R^2 = 0.7619$), 20% sucrose (F (DFn, DFd) = 2.143 (1, 1), $P = 0.3815$, $R^2 = 0.6819$), and 30% sucrose (F (DFn, DFd) = 2.964 (1, 1), $P = 0.3350$, $R^2 = 0.7477$). The elevation of each line was significantly different (F (DFn, DFd) = 335,726 (2, 5), $P < 0.0001$) and given as follows: 10%: 1.325 (95% CI: 1.274—1.371), 20%: 1.911 (95% CI: 1.887 to 1.959), and 30%: 3.184 (95% CI: 3.171 to 3.19).

3.4 The Contribution of the Stored [PLT] to PC Fluid Viscosity

Linear regression was used to test if the stored [PLT] significantly influenced the Newtonian characteristics of the suspension (Fig. 6A). It was found that the [PLT] did not significantly influence the measured PC fluid viscosity over a range of shear rates, measured by co-stream microfluidics. The overall regression showed the slope did not deviate significantly from zero for PCs stored at 0.5x [PLT], 1x [PLT], and 2x [PLT]. Similarly, no significant slopes were shown at any [PLT] suspended in PAS. A comparison between the elevation/intercepts of the PLT suspensions showed the differences to be significant (F (DFn, DFd) = 3446 (5, 11), $P < 0.0001$). Likewise, no significant difference was shown as [PLT] increased in both PC and PAS suspensions measured by NTM; however, at all stored [PLTs], there was a significant difference in the viscosity of PLTs suspended in PC compared to PLTs suspended in PAS (Fig. 6B). This suggests PC viscosity is greater influenced by the suspension media rather than the [PLT].

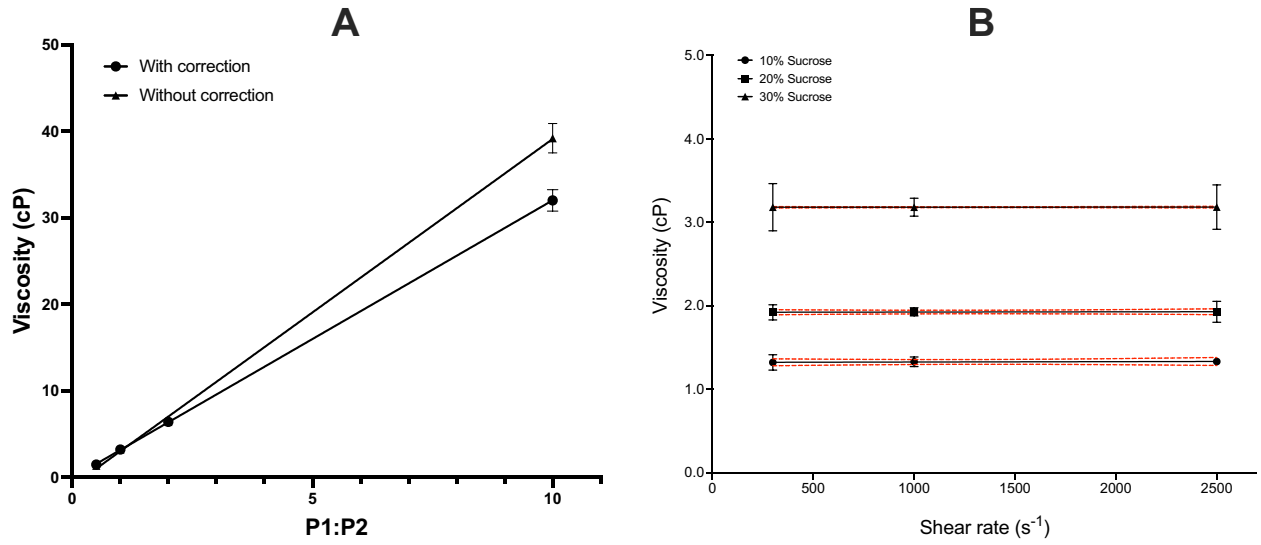

Fig. 5 Co-stream microfluidic model validation for rheological characterisation. (**A**) linear regression analysis with and without the application of Eq. 2.4, illustrating the model's predictive performance. (**B**) Viscosity measurements of sucrose suspensions (10–30%; w/wt) at a range of shear rates. The black line denotes the fitting lines given by linear regression, and the 95% confidence intervals are represented by the red dotted line. Data is presented as mean values with error bars representing standard deviation (SD)

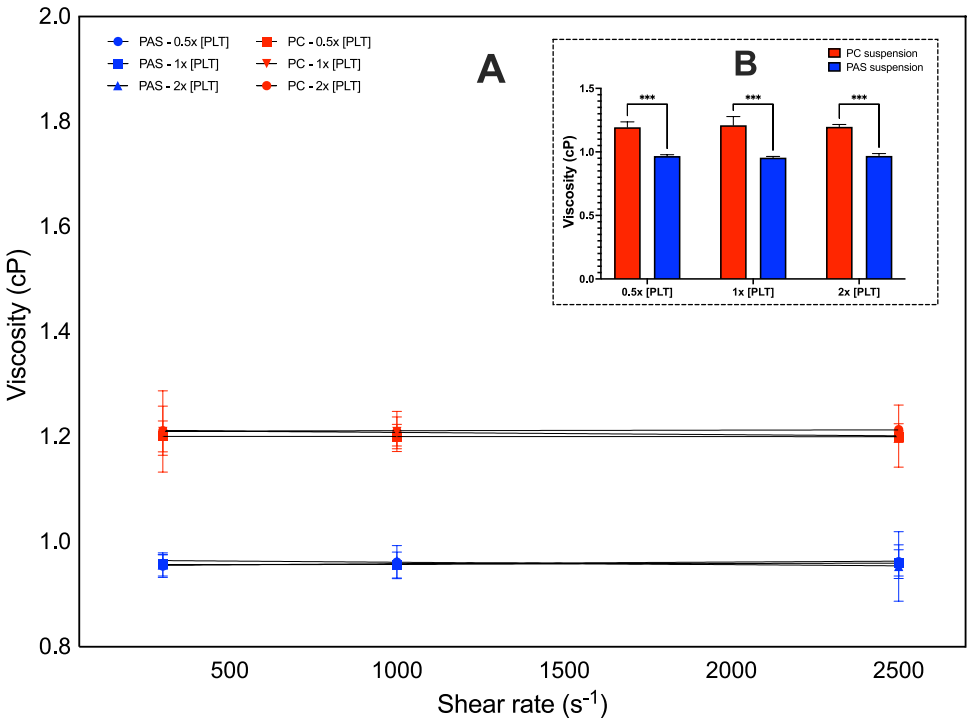

Fig. 6 The effect of [PLT] on PC fluid viscosity. (**A**) shows the dependency of [PLT] in either PC or PAS suspension on the fluid viscosity at a range of shear rates ($n=3$) measured using co-stream microfluidics. Fitting lines denote results from linear regression analysis. (**B**) illustrates the viscosity measured using NTM of PLT suspensions suspended in PC (red bars) or PAS (black bars). Data is presented as mean values with error bars representing SD ($N=4$). Significance was inferred by a two-way ANOVA followed by a post hoc Tukey's test with significance denoted as follows: ***=$P<0.001$

3.5 The Contribution of Residual Plasma to PC Fluid Viscosity

Linear regression was used to test if residual plasma significantly influenced the Newtonian characteristics of PC suspensions. It was found that residual plasma content did not significantly influence the PC fluid viscosity over a range of shear rates, measured by co-stream microfluidics (Fig. 7A). The regression analysis showed the slope did not deviate significantly from zero for PCs stored in 100% plasma, 1:3 PAS:plasma, 1:1 PAS:plasma, 3:1 PAS:plasma, and 100% PAS. A comparison of fits between the slopes for each residual plasma content showed the differences to not be significant (F (DFn, DFd)=1.540. (4, 5), $P=0.3197$) and a comparison of fits between the elevation/intercepts showed the differences to be significant (F (DFn, DFd)=2220 (4, 9), $P<0.0001$).

Non-linear regression was then used to test how the residual plasma content influences the PC fluid viscosity, measured by co-stream microfluidics (Fig. 7B). It was found that residual plasma shows a non-linear relationship to fluid viscosity, independent of the applied shear rate, following a second order polynomial curve ($y=B0+B1x+B2x^2$). A comparison of fits between the curves fitted for each shear rate showed the differences between the slopes to not be significant (F (DFn, DFd)=0.1220 (6, 6), $P=0.9891$); therefore, all data can be represented by one curve. The shared best fit values were as follows: B0=0.9724 (95% CI=0.9346 - 1.010), B1=0.9365 (95% CI=0.7574 - 1.116), and B2=−0.4843 (95% CI=−0.6560 - - 0.3125). Overall, the regression showed a good fit for 300 s^{-1} ($R^2=0.9722$), 1000 s^{-1} ($R^2=0.9819$), and 2500 s^{-1} ($R^2=0.9606$).

The Individual variation for each FFP sample (labelled N1 to N3) was measured by co-stream microfluidics and assessed by linear regression (Fig. 7C). It was found that donor variability influenced the measured plasma viscosity, independent of shear rate. A comparison of fits between the slopes for each sample showed the differences to not be significant (F (DFn, DFd)=2.222 (2, 3), $P=0.2559$). The regression analysis showed variable R^2 values: N1 ($R^2=0.4200$), N2 ($R^2=0.8799$), and N3 ($R^2=0.2958$). However, a comparison of fits between the intercepts/elevations of each sample showed the differences to be significant (F (DFn, DFd)=24.05, (2, 5), $P=0.0027$).

3.6 Influence of Reduced Residual Plasma on PLT Quality Over Storage

The impact of decreasing residual plasma content on PC quality over storage was evaluated by assessing changes in [PLT] and pH (Fig. 8A, B). By day 8, only the 0% plasma group showed a significant decrease in [PLT] compared to the control (355 plasma; $P<0.001$). However, when comparing day 1 to day 8 within each group, a significant decrease was observed in the 0% ($P<0.001$), 5% ($P<0.01$), and 10% ($P<0.01$) plasma groups. 15% plasma and the control remained stable across the storage duration. In contrast, all reduced plasma groups (0%, 5%, 10%, and 15%) showed

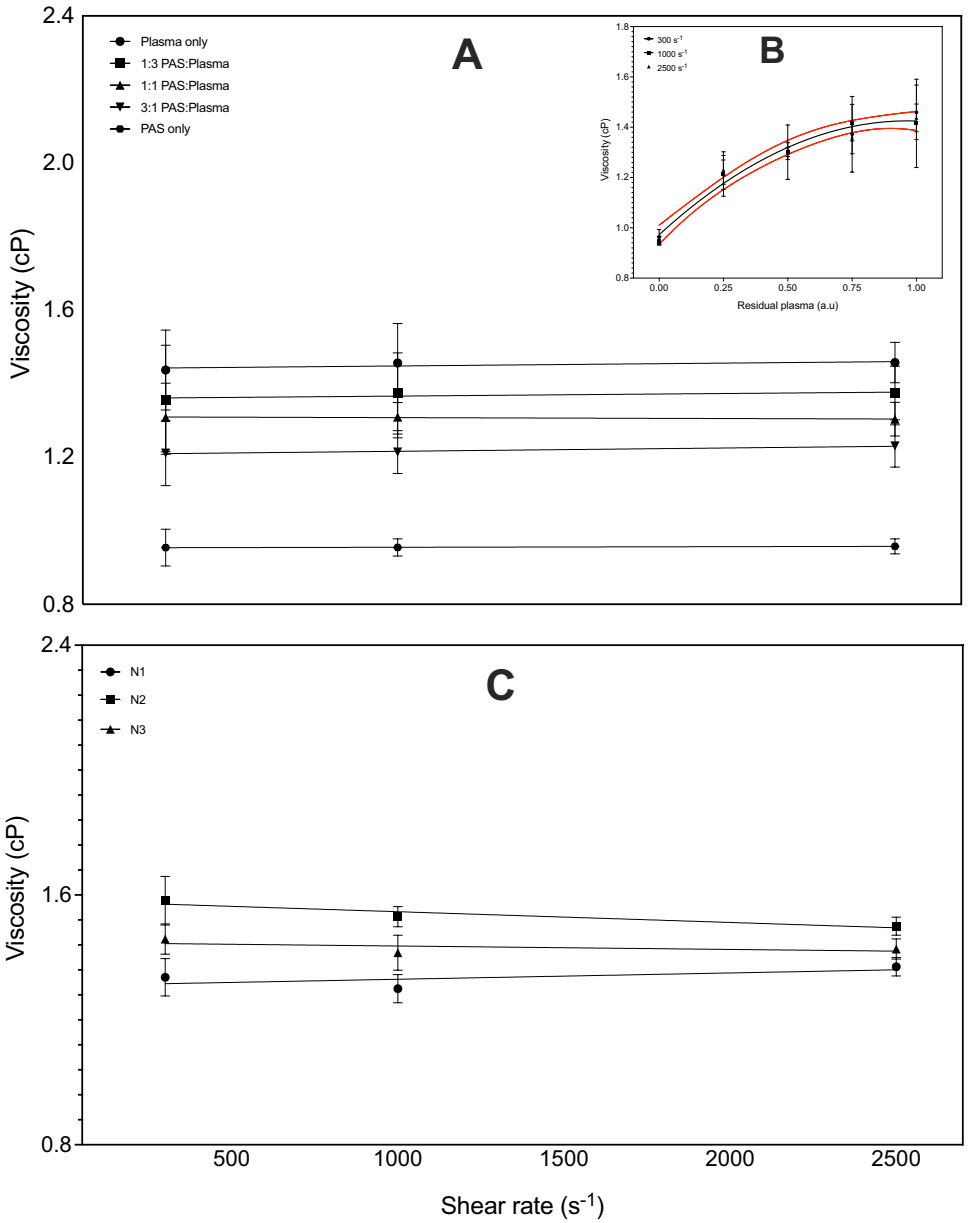

Fig. 7 The influence of residual plasma on PC fluid viscosity. Fluid viscosity was measured using co-stream microfluidics. (**A**) Shows the dependency of residual plasma on the fluid viscosity at a range of shear rates ($N=3$), with black lines represent fitting lines given from linear regression analysis. (**B**) shows the relationship between relative residual plasma and viscosity at 300 s^{-1} ($N=3$), with black lines representing fitting lines given from non-linear regression and dashed red lines representing 95% CI. (**C**) shows the individual measurement variation for each FFP sample (100% plasma) recorded in triplicate, with N1, N2, and N3 representing individual FFP samples. Black lines represent fitting lines given from linear regression analysis. Data is presented as mean values with error bars representing SD

significantly lower pH values compared to the control (35% plasma; all $P<0.001$) on day 8 of storage (Fig. 8B). When comparing day 1 to day 8 within each group, pH was stable in the control, while significant decreases were observed in the 0% ($P<0.0001$), 5% ($P<0.0001$), 10%, ($P<0.01$), and 15% ($P<0.001$) plasma groups. Despite these differences, pH values in all groups remained within acceptable limits recommended by the JPAC storage guidelines [28].

PLT morphology during storage was inferred from changes in MPV and PDW (Fig. 8C, D). MPV was significantly increased in the 0% ($P<0.001$) and 5% ($P<0.0001$) plasma groups by day 8 of storage compared to the control, with no significant differences observed in the 10%, or 15% plasma groups (Fig. 8C). Over the storage period, MPV was unchanged in 10%, 15%, and the control plasma groups, while significant increases were shown in the 0% ($P<0.001$), and 5% ($P<0.0001$) plasma groups. Similarly, PDW was significantly elevated in the 5% plasma group ($P<0.05$) compared to the control on day 8 (Fig. 8D). However, within-group comparisons over time did not show significant changes in PDW from day 1 to day 8 in any group.

PLT function was assessed using TRAP-6 and ristocetin induced aggregation (Fig. 9A, B). A significant decrease in TRAP-6 induced aggregation was observed in the 10% plasma group compared to the control on day 8 ($P<0.05$; Fig. 9A). Over storage, TRAP-6 induced aggregation decreased in both 15% ($P<0.05$) and 10% ($P<0.01$) plasma groups by day 8 compared to day 2, whereas the

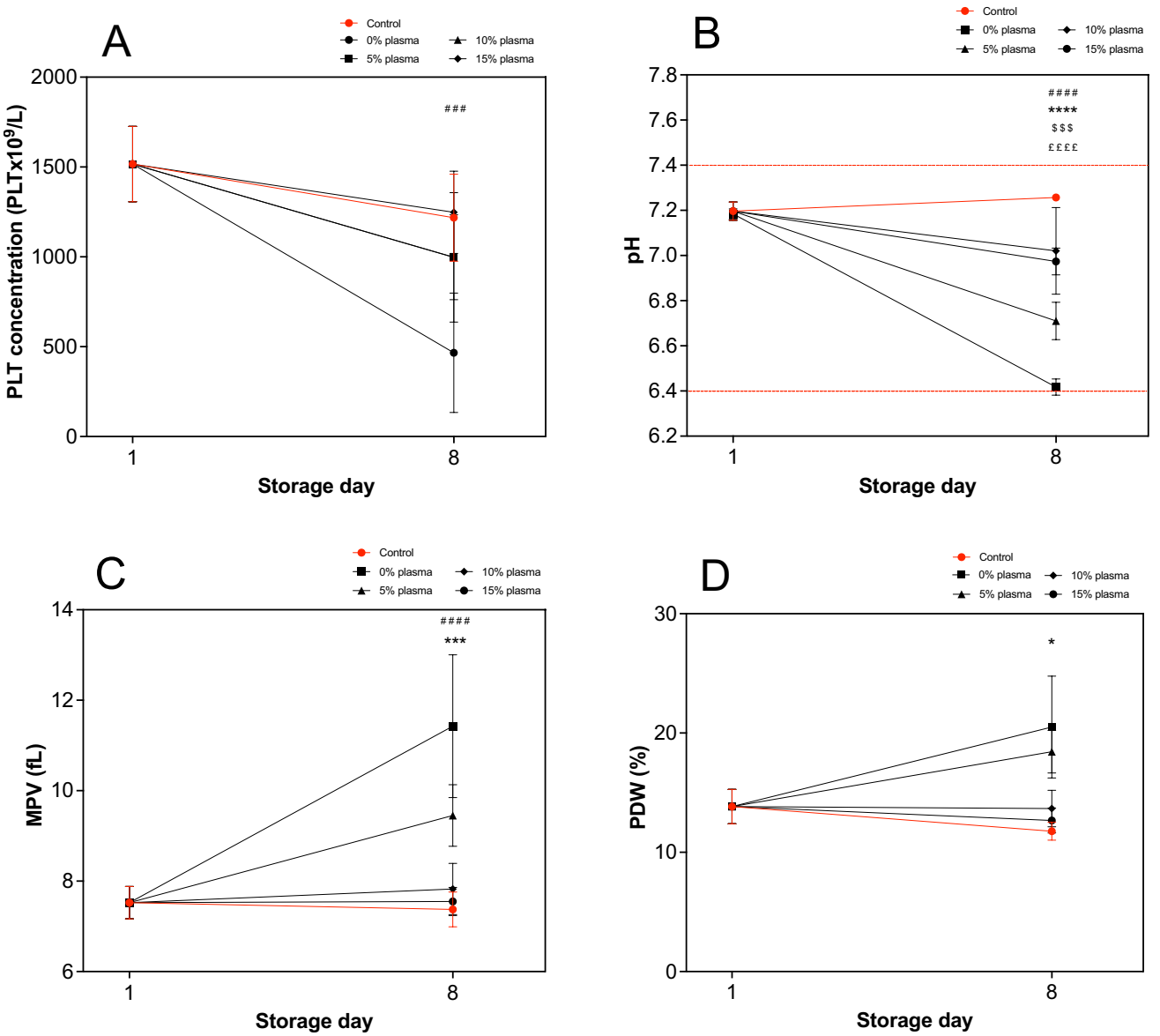

Fig. 8 Viability, MPV, and pH of PCs stored with reduced plasma. PCs were suspended in varying plasma fractions, from 0 to 35% plasma. Red line on each graph represents the control (35% plasma). (**A**) represents the change in [PLT], (**B**) represents the change in pH, (**C**) represents the change in MPV, and (**D**) represents the change in PDW, over 8 days of storage. The dotted red lines represent the boundaries given by the UK guidelines [28]. Graphs show mean values with error bars representing SD ($N=4$). Significance was inferred by a two-way ANOVA followed by a Dunnett's post hoc test. Significance was denoted as follows: ££££$=P<0.0001$ for 15% and control (35%) comparisons; \$\$\$$=P<0.001$ for 10% and control (35%) comparisons; *$=P<0.05$, ***$=P<0.001$, ****$=P<0.0001$ for 5% and control (35%) comparisons; ###$=P<0.001$, ####$=P<0.0001$ for 0% and control (35%) comparisons

control showed no significant decrease in TRAP-6 induced aggregation over the storage duration. In contrast, Ristocetin induced aggregation remained consistent across groups and time points, with no significant differences observed between plasma groups or between storage days (Fig. 9B).

PLT activation was then evaluated using CD62P and CD42b expression (Fig. 9C, D). No significant differences in CD62P expression were observed between groups on any storage day (Fig. 9C). However, a significant increase in CD62P expression on day 8 compared to day 2 was observed in the 15% plasma group ($P<0.05$), while the control and 10% plasma remained stable over storage. Similarly, CD42b expression showed no significant differences between groups on any day (Fig. 9D). Although a significant decrease in CD42b expression was shown in the control group on day 8 relative to day 2 ($P<0.05$), no significant changes were observed in the 10%, or 15% plasma groups over storage.

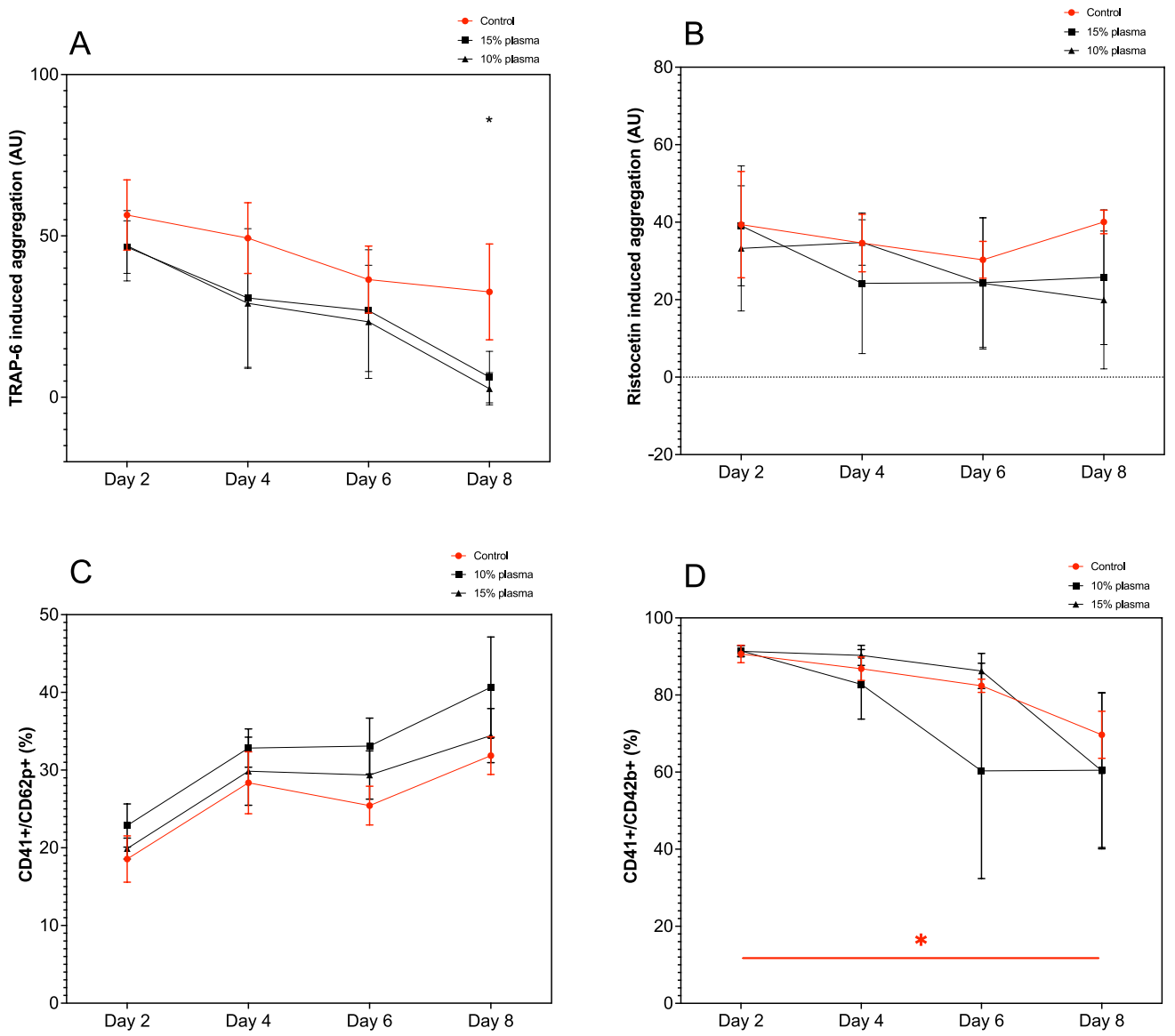

Fig. 9 Functionality and surface expression of PCs stored with reduced plasma. PCs were suspended in varying plasma from 0 to 35% plasma. Red line on each graph represents the control (35% plasma). (**A**) and (**B**) represents the change in agonist induced aggregation in response to TRAP-6 and Ristocetin, respectively, while (**C**) and (**D**) represent the change in CD41 +/CD62p + and CD41 +/CD42b + expression, respectively, over 8 days of storage. Graphs show mean values with error bars representing SD ($N=4$).Significance was inferred by a two-way ANOVA followed by a Tukey's post hoc test. Significance was denoted as follows: * = $P<0.05$ for 10% and control (35%) comparisons

4 Discussion

Fluid viscosity plays a critical role in the dynamics of both physical and biological systems, determining the shape of flow distribution and providing an indicator for further fluid material properties [33]. This study aimed to characterise the rheological properties of stored PCs to highlight areas which could address the Si-PSL and help optimise the therapeutic PC product for neonatal transfusion. Firstly, the study proposed two models to measure the viscosity of biological suspensions, NTM and co-stream microfluidics. The former suspended fluorescent polyethylene beads within the test sample and predicted the viscosity using the apparent measured bead diameter to the actual bead diameter (Fig. 1), while the latter used the location of the fluid interface between the reference and test sample flow to determine the fluid viscosity (Fig. 2). Sucrose suspensions from 0–30% (w/wt) were used to evaluate the effectiveness of both models in predicting fluid viscosity. Sucrose suspensions were used as they demonstrate a constant viscosity independent of shear rate and have been well characterised previously

[37, 38]. The results indicated that both methods can accurately measure the viscosity of test samples, with the co-stream microfluidic method demonstrating slightly higher measurement precision, reflected by narrower confidence intervals (Fig. 5). Beyond quantitative accuracy, each technique presents unique operational advantages. The NTM approach offers benefits in ease of use, potential for automation, and minimal sample preparation, whereas the co-stream microfluidic platform allows rapid viscosity measurement across a range of shear rates and may offer improved precision under controlled flow conditions, providing complementary information on fluid rheology.

The study identified that changes to the stored [PLT] did not influence the viscosity of the PC and maintained the rheological characteristics of the suspension media. This result contrasts with the findings of Mitra et al. [29], which reported shear-thinning behaviour in PRP samples [29]. This discrepancy may be attributed to differences in the volume fraction occupied by various cell types within the suspension. The study by Mitra et al. [29], reported total volume fractions up to 13.56%, and RBC contamination levels as high as 12.54%[29]. Given that PCs for transfusion are typically stored at a total cellular volume fraction of < 1.5% (Table 1), our results better reflect the rheological context relevant to transfusion practice. RBCs are known to significantly influence the rheological properties of suspensions due to their mechanical properties, which facilitate cell–cell interactions, deformation and alignment under shear flow, resulting in reduced apparent viscosity with increasing shear rates [39]. In contrast, the low total cellular volume fraction of PCs likely accounts for the rheological properties being primarily governed by the suspension media, independent to the stored [PLT] (Fig. 6).

A key finding of this study was the non-linear relationship between residual plasma content and the viscosity of PC suspensions, which was consistent at all tested shear rates (300, 1000, 2500 s^{-1}; Fig. 7A, B). This suggests that PC viscosity is independent of shear induced behaviours and instead influenced by intrinsic changes in the fluid microstructure, likely driven by concentration-dependent interactions between plasma proteins. Plasma contains several high molecular weight components, such as fibrinogen, immunoglobins and lipoproteins, which can interact to form dynamic networks, especially at increasing concentrations [40]. These interactions may amplify viscous resistance in a non-linear manner, contributing to the disproportionate increase in the rheological properties of the suspension. This trend is further emphasised by the observed influence of donor variability on the viscosity of FFP samples (Fig. 7C), highlighting the inter-individual differences in plasma composition. In contrast, viscosity measurements of BC derived PCs showed minimal variation between units. This difference is likely due to the pooling of four buffy coat donations during manufacturing, which may buffer individual differences. However, apheresis derived PCs may be more susceptible to donor dependent variability in viscosity, as they are manufactured from single donor units. It would therefore be valuable to investigate whether viscosity correlates with quality parameters in apheresis derived PCs.

Considering the above findings, reduced plasma strategies were further explored as a means of addressing the Si-PSL. The current study revealed that reducing plasma to ≥ 10% in PC storage has no significant impact on PLT viability or morphology. However, reducing plasma below this threshold resulted in a significant decrease in [PLT] and a significant increase in MPV and PDW by day 8 of storage (Fig. 8), indicating PLT degradation and compromised structural integrity. These findings align with previous work by Gravemann et al. [41], which similarly reported a minimum residual plasma concentration of ≥ 10% required to maintain cell viability [41]. These findings differ from a study described in a review by Van der Meer [18], which reported no significant differences in PC quality when stored with 100% PAS (SSP + with glucose), compared to PCs stored with 65%:35% PAS (SSP +) to plasma ratio [18]. However, it is important to note that the study referenced remains unpublished, limiting the ability to directly compare methodologies and outcomes. In the present study, dextrose monohydrate was also supplemented in the reduced plasma groups; still, a marked deterioration in PLT morphology was observed when residual plasma fell below 10%. This suggests glucose alone is insufficient in maintaining PC quality at low plasma concentration, and that other plasma-derived components are essential for preserving PLT viability and structural stability over storage.

Further analysis investigating functionality and activation status of PCs stored with ≥ 10% plasma showed PLT function was largely preserved under these conditions (Fig. 9). TRAP-6 induced aggregation, which reflects thrombin receptor pathway responsiveness [42], showed a modest but significant reduction in the 10% plasma group compared to the control of day 8. Additionally, both the 10% and 15% plasma groups showed a significant decline in TRAP-6 responsiveness over storage, suggesting some time dependent functional deterioration. On the other hand, Ristocetin induced aggregation remained stable across all groups, suggesting preserved GPIb-von Willebrand factor responsiveness [42]. Markers of PLT activation, P-selectin (CD62P), and GPIbα (CD42b), showed minimal changes over storage in PCs with ≥ 10% plasma. CD62P expression was generally stable, with only the 15% plasma group showing a significant decline by day 8 (Fig. 9C). CD42b expression also remained stable in the reduced plasma

groups, with a significant decrease observed only in the control (Fig. 9D). This observation supports the hypothesis that viscosity may influence shear-induced receptor shedding as part of the Si-PSL. However, the preservation of CD42b in the reduced plasma groups, despite a decrease in TRAP-6 induced aggregation, suggests that while viscosity may play a role in receptor shedding, another component of plasma appears to be critical for maintaining overall PC quality.

NTM provides high sensitivity in measuring the motion of nanoparticles within a fluid to infer the rheological properties of biological suspensions. This method provides some advantages over conventional rheometers, including simple calibration, easy use, and relatively small sample volumes for analysis; however, NTM does have some limitations. NTM is primarily effective for dilute, transparent or semi-transparent fluids, as the technique relies on the tracking of particles through light scattering. Likewise, biological fluids also often containing submicron particles, including exosomes and microvesicles, which can influence the measured bead size distribution. The addition of an ultracentrifugation step was thus used to ensure only beads were tracked in the analysis. The NTM model also imposed a fixed flow rate, so viscosity measurements were fixed to a single shear rate.

To ensure accuracy of fluid viscosity measurements of biological suspensions, such as PC and FFP, and to determine the dependency of shear rate on fluid viscosity, the co-stream microfluidic method was used alongside NTM. The co-stream microfluidic method relies both on laminar flow between the two fluids as well as the visual clarity at the interface. To enhance the visual clarity of the interface, the reference fluid (PBS) was stained with < 0.001% Trypan Blue. This did not alter the viscosity of the fluid; however, as both fluids used in this study are miscible, it is possible diffusional smearing of the fluid interface can occur. To minimise diffusional smearing at the fluid interface, both the Reynolds number (Re), and Peclet number (Pe) were considered in the fabrication of the microfluidic device. Re is a numerical value defining whether the flow is predominately inertial or viscous flow. Laminar flow is expected when the Reynolds number is < 2300 [14, 43]. Similarly, Pe is a numerical value defining whether the fluid flux is driven by bulk flow (advection), or by diffusion. Advective flow is expected to predominate with a Peclet number > 1 [27]. Another limitation with the study is due to the small sample size and inter-donor variation between samples. However, for PC viscosity this was addressed by using a pooled and split protocol.

Temperature is a well-established factor influencing viscosity and viscoelastic properties [44]. While both the NTM and co-stream microfluidic methods used in this study can be adapted for temperature-controlled measurements, using microscope heating stages, our present work focused on PCs stored under standard room temperature, agitated conditions, which represent current clinical storage practice. Cold storage studies were not undertaken, as these conditions, typically unagitated and at 4 °C, differ substantially in handling and relevance to the Si-PSL [45]. Nevertheless, both NTM and co-stream microfluidics are technically compatible with future investigations into temperature dependent rheological behaviour.

To conclude, this study showed both NTM and co-stream microfluidics are effective methods in measuring fluid viscosity of biological fluids. Notably, the co-stream microfluidic model enabled viscosity assessment across a range of physiologically relevant shear rates. PC viscosity was shown to be dependent on the residual plasma following processing, but independent to the stored [PLT]. Reducing plasma to 10% largely maintained PC quality over 8 days storage, but further reductions led to reduced [PLT] and increased MPV. Future studies should aim to identify the specific plasma component that confers structural and functional stability over PC storage. Understanding these mechanisms could support the development of improved additive solutions that both preserve PLT integrity and effectively address the Si-PSL.

Author Contributions DP designed the research study, performed the research, acquired and analysed the data, and wrote the first draft of the manuscript; A.D, J.O, C.S, C.G, and P.J supervised the research. A.P, A.D, J.O, C.S, C.G, and P.J and reviewed and edited the manuscript.

Funding Dean Pym was in receipt of a joint PhD scholarship between the Welsh Blood Service and Cardiff Metropolitan University.

Data Availability The authors affirm that all data supporting the findings of this study are included in the article.

Declarations

Ethics Declaration Not applicable.

Competing interests The authors declare no competing interests.

References

1. Shrivastava, M. (2009). The platelet storage lesion. *Transfusion and Apheresis Science, 41*(2), 105–113. https://doi.org/10.1016/j.transci.2009.07.002
2. Sturk, A., Burt, L. M., Hakvoort, T., ten Cate, J. W., & Crawford, N. (1982). The effect of storage on platelet morphology. *Transfusion, 22*(2), 115–120. https://doi.org/10.1046/j.1537-2995.1982.22282177116.x
3. Özpolat T, Yakovenko O, Stratiievska A, Bailey SL, Miles J, Usaneerungrueng C, Byrne D, Wu X, Stolla M. (2023). Evaluating stored platelet shape change using imaging flow cytometry. *Platelets*, *34*(1), 2136646. https://doi.org/10.1080/09537104.2022.2136646
4. Rinder, H. M., & Snyder, E. L. (1992). Activation of platelet concentrate during preparation and storage. *Blood Cells, 18*(3), 445–456. discussion 457–460.
5. Escolar, G., & McCullough, J. (2019). Platelet in vitro assays: Their correspondence with their in vivo hemostatic potential. *Transfusion, 59*(12), 3783–3793. https://doi.org/10.1111/trf.15559
6. Kiouptsi, K., Gambaryan, S., Walter, E., Walter, U., Jurk, K., & Reinhardt, C. (2017). Hypoxia impairs agonist-induced integrin αIIbβ3 activation and platelet aggregation. *Scientific Reports, 7*(1), 7621. https://doi.org/10.1038/s41598-017-07988-x
7. Montague, S. J., Andrews, R. K., & Gardiner, E. E. (2018). Mechanisms of receptor shedding in platelets. *Blood, 132*(24), 2535–2545. https://doi.org/10.1182/blood-2018-03-742668
8. Cheng, L., Lu, W., Shichun, W., Qi, L., Ronghua, D., & Yao, C. (2025). The effect of physical cues on platelet storage lesion. *Hematology, 30*(1), 2450573. https://doi.org/10.1080/16078454.2025.2450573
9. Wang, S., Liu, Q., Cheng, L., Wang, L., Xu, F., & Yao, C. (2022). Targeting biophysical cues to address platelet storage lesions. *Acta Biomaterialia, 151*, 118–133. https://doi.org/10.1016/j.actbio.2022.08.039
10. Di Stasio, E., & De Cristofaro, R. (2010). The effect of shear stress on protein conformation: Physical forces operating on biochemical systems: The case of von Willebrand factor. *Biophysical Chemistry, 153*(1), 1–8. https://doi.org/10.1016/j.bpc.2010.07.002
11. Greene, J. P. (2021). 5 - rheology and plastic flow. In J. P. Greene (Ed.), *Automotive plastics and composites* (pp. 57–69). William Andrew Publishing. https://doi.org/10.1016/B978-0-12-818008-2.00001-5
12. Sharma, P. K. (2010). Mechanics of materials. *Technology and Health Care, 18*(1), 49–61. https://doi.org/10.3233/thc-2010-0566
13. Casa, L. D. C., Deaton, D. H., & Ku, D. N. (2015). Role of high shear rate in thrombosis. *Journal of Vascular Surgery, 61*(4), 1068–1080. https://doi.org/10.1016/j.jvs.2014.12.050
14. Pym, D., Davies, A. J., Williams, J. O., Saunders, C., George, C. E., & James, P. E. (2024). Small volume platelet concentrates for neonatal use are more susceptible to shear-induced storage lesion. *Platelets, 35*(1), 2389967. https://doi.org/10.1080/09537104.2024.2389967
15. Schoenfeld, H., Muhm, M., Doepfmer, U. R., Kox, W. J., Spies, C., & Radtke, H. (2005). The functional integrity of platelets in volume-reduced platelet concentrates. *Anesthesia and Analgesia, 100*(1), 78–81. https://doi.org/10.1213/01.ane.0000140239.43116.30
16. Shankaran, H., Alexandridis, P., & Neelamegham, S. (2003). Aspects of hydrodynamic shear regulating shear-induced platelet activation and self-association of von Willebrand factor in suspension. *Blood, 101*(7), 2637–2645. https://doi.org/10.1182/blood-2002-05-1550
17. Gulliksson, H. (2014). Platelet storage media. *Vox Sanguinis, 107*(3), 205–212. https://doi.org/10.1111/vox.12172
18. van der Meer, P. F. (2016). PAS or plasma for storage of platelets? A concise review. *Transfusion Medicine, 26*(5), 339–342. https://doi.org/10.1111/tme.12325
19. Salazar Vázquez, B. Y., Cabrales, P., Tsai, A. G., & Intaglietta, M. (2011). Nonlinear cardiovascular regulation consequent to changes in blood viscosity. *Clinical Hemorheology and Microcirculation, 49*(1–4), 29–36. https://doi.org/10.3233/ch-2011-1454
20. Sloop, G. D., De Mast, Q., Pop, G., Weidman, J. J., & St Cyr, J. A. (2020). The role of blood viscosity in infectious diseases. *Cureus, 12*(2), e7090. https://doi.org/10.7759/cureus.7090
21. Srivastava, N., & Burns, M. A. (2006). Analysis of non-Newtonian liquids using a microfluidic capillary viscometer. *Analytical Chemistry, 78*(5), 1690–1696. https://doi.org/10.1021/ac0518046
22. Sutera, S. P., Nowak, M. D., Joist, J. H., Zeffren, D. J., & Bauman, J. E. (1988). A programmable, computer-controlled cone-plate viscometer for the application of pulsatile shear stress to platelet suspensions. *Biorheology, 25*(3), 449–459. https://doi.org/10.3233/bir-1988-25306
23. Doffin, J., Perrault, R., & Garnaud, G. (1984). Blood viscosity measurements in both extensional and shear flow by a falling ball viscometer. *Biorheology. Supplement, 1*, 89–93. https://doi.org/10.3233/bir-1984-23s114
24. Ahuja, A., Lee, R., & Joshi, Y. M. (2021). Advances and challenges in the high-pressure rheology of complex fluids. *Advances in Colloid and Interface Science, 294*, 102472. https://doi.org/10.1016/j.cis.2021.102472
25. Varlet-Marie, E., & Brun, J. F. (2011). Prediction of RBC aggregability and deformability by whole body bioimpedance measurements analyzed according to Hanai's mixture conductivity theory. *Clinical Hemorheology and Microcirculation, 47*(2), 151–161. https://doi.org/10.3233/ch-2010-1378
26. Salipante, P. F., Kuei, S., & Hudson, S. D. (2022). A small-volume microcapillary rheometer. *Rheologica Acta*. https://doi.org/10.1007/s00397-022-01333-4
27. Gupta, S., Wang, W. S., & Vanapalli, S. A. (2016). Microfluidic viscometers for shear rheology of complex fluids and biofluids. *Biomicrofluidics, 10*(4), 043402. https://doi.org/10.1063/1.4955123
28. JPAC. Chapter 5.7: Whole blood donation. Retrieved 24 October 2024 from https://www.transfusionguidelines.org [Last Accessed 28 July 2025].
29. Mitra, H., Jayaram, P., Bratsman, A., Gabel, T., & Alba, K. (2020). Characterization and rheology of platelet-rich plasma. *Journal of Rheology, 64*(5), 1017–1034. https://doi.org/10.1122/1.5127743
30. Gardiner, C., Ferreira, Y. J., Dragovic, R. A., Redman, C. W., & Sargent, I. L. (2013). Extracellular vesicle sizing and enumeration by nanoparticle tracking analysis. *Journal of Extracellular Vesicles*. https://doi.org/10.3402/jev.v2i0.19671
31. Gross, J., Sayle, S., Karow, A. R., Bakowsky, U., & Garidel, P. (2016). Nanoparticle tracking analysis of particle size and concentration detection in suspensions of polymer and protein samples: Influence of experimental and data evaluation parameters. *European Journal of Pharmaceutics and Biopharmaceutics, 104*, 30–41. https://doi.org/10.1016/j.ejpb.2016.04.013
32. Saveyn, H., De Baets, B., Thas, O., Hole, P., Smith, J., & Van der Meeren, P. (2010). Accurate particle size distribution determination by nanoparticle tracking analysis based on 2-D Brownian dynamics simulation. *Journal of Colloid and Interface Science, 352*(2), 593–600. https://doi.org/10.1016/j.jcis.2010.09.006
33. Hong, H., Song, J. M., & Yeom, E. (2019). 3D printed microfluidic viscometer based on the co-flowing stream. *Biomicrofluidics, 13*(1), 014104. https://doi.org/10.1063/1.5063425
34. Yeom, E., Park, J. H., Kang, Y. J., & Lee, S. J. (2016). Microfluidics for simultaneous quantification of platelet adhesion and blood viscosity. *Scientific Reports, 6*, 24994. https://doi.org/10.1038/srep24994

35. Schindelin, J., Arganda-Carreras, I., Frise, E., Kaynig, V., Longair, M., Pietzsch, T.,..., & Cardona, A. (2012). Fiji: An open-source platform for biological-image analysis. *Nature Methods*, *9*(7), 676–682. https://doi.org/10.1038/nmeth.2019
36. Decaux, O., Laurat, E., Perlat, A., Cazalets, C., Jego, P., & Grosbois, B. (2009). Systemic manifestations of monoclonal gammopathy. *European Journal of Internal Medicine, 20*(5), 457–461. https://doi.org/10.1016/j.ejim.2009.01.001
37. Swindells, J. F., Snyder, C. F., Hardy, R. C., & Golden, P. E. (1958). *Viscosities of sucrose solutions at various temperatures: Tables of recalculated values*. For sale by the Supt. of Docs., U.S. G.P.O.
38. Telis, V. R. N., Telis-Romero, J., Mazzotti, H. B., & Gabas, A. L. (2007). Viscosity of aqueous carbohydrate solutions at different temperatures and concentrations. *International Journal of Food Properties, 10*(1), 185–195. https://doi.org/10.1080/10942910600673636
39. Gillespie, A. H., & Doctor, A. (2021). Red blood cell contribution to hemostasis. *Frontiers in Pediatrics, 9*, 629824. https://doi.org/10.3389/fped.2021.629824
40. Nair, C. H., & Dhall, D. P. (1991). Studies on fibrin network structure: The effect of some plasma proteins. *Thrombosis Research, 61*(3), 315–325. https://doi.org/10.1016/0049-3848(91)90109-a
41. Gravemann, U., Volgmann, T., Min, K., Philipp, R., Lambrecht, B., Müller, T. H., & Seltsam, A. (2015). In vitro variables of buffy coat-derived platelet concentrates with residual plasma of down to 10% are stably maintained in new-generation platelet additive solutions. *Transfusion, 55*(7), 1700–1709. https://doi.org/10.1111/trf.13000
42. Paniccia, R., Priora, R., Liotta, A. A., & Abbate, R. (2015). Platelet function tests: A comparative review. *Vascular Health and Risk Management, 11*, 133–148. https://doi.org/10.2147/vhrm.s44469
43. Torres, R., Tormey, C. A., & Stack, G. (2016). Fluid motion and shear forces in platelet storage bags with different modes of agitation. *Vox Sanguinis, 111*(2), 209–212. https://doi.org/10.1111/vox.12409
44. Peleg, M. (2018). Temperature-viscosity models reassessed. *Critical Reviews in Food Science and Nutrition, 58*(15), 2663–2672. https://doi.org/10.1080/10408398.2017.1325836
45. Shea, S. M., Spinella, P. C., & Thomas, K. A. (2022). Cold-stored platelet function is not significantly altered by agitation or manual mixing. *Transfusion, 62*(9), 1850–1859. https://doi.org/10.1111/trf.17005